Proceedings of the 18th International Symposium on the Packaging and Transportation of Radioactive Materials
PATRAM 2016
September 18-23, 2016, Kobe, Japan

Paper No.2010

Study on Temperature Estimation Method of PWR Spent Fuel Cladding in Dry Storage

Hideki Yagihashi, Jiro Katayama, Masakiyo Hishida

Regulatory Standard and Research Department,
Secretariat of Nuclear Regulation Authority (S/NRA/R),
Tokyo, Japan

Abstract

In the Recyclable Fuel Storage Center, which is the first away from reactor (AFR) spent fuel storage facility in Japan, spent nuclear fuel (SNF) from BWRs and PWRs is scheduled to be stored in Dual Purpose Casks (DPCs). In the case of DPC storage in this center, if no abnormality in the external appearance or the inter-lid pressure of DPC is found during the storage period, the DPC and the stored fuel will be considered to be intact throughout the storage period, and the DPC will be shipped without opening its lids for pre-shipment inspection. Therefore, integrity of stored fuel during storage should be confirmed without opening DPC lids. Creep deformation and hydride reorientation are considered as major deterioration mechanisms of fuel cladding during dry storage, and they depend on the cladding temperature history. In this paper we focus on the fuel cladding temperature change during a long-term storage test using a test container which can store two PWR SNF bundles, conducted by the electric utilities in advance of the commissioning of actual storage at the Recyclable Fuel Storage Center, and present a result of the review for the temperature prediction performance of the analysis model which we developed as an approach for fuel cladding temperature estimation by measuring the surface temperature of test container. The performance of the model was reviewed by comparing the analysis results with the measured temperature distributions of the test container in the preliminary heat transfer test.

1. Introduction

The Japan's first AFR dry storage facility for SNF, the Recyclable Fuel Storage Center in Mutsu-shi, Aomori, has completed its construction, and dry storage of BWR and PWR SNF by using DPCs is under safety review based on the new regulatory requirements. In this center, if there is no mechanical impact such as DPC overturning or fluctuation of the inter-lid pressure during the storage period, integrity of DPC and stored fuel is considered to be maintained throughout the storage period, and DPC will be shipped without opening DPC lids for pre-shipment inspection. So the evaluation for integrity of stored SNF is one of the core technologies for DPC storage.

Japan has experiences of at reactor (AR) BWR SNF dry storage in metal casks and of the integrity check of the stored BWR SNF by opening DPC lids. Meanwhile, due to the lack of PWR SNF dry storage experience, the electric utilities planned a long-term storage test campaign in advance of the start of actual storage at the Recyclable Fuel Storage Center. In this test, 42.8 GWd/t and 55 GWd/t SNF bundles are to be stored in the test container; 42.8 GWd/t SNF bundle is to be stored from the beginning of the test and 55 GWd/t SNF bundle will be added from 10 years after the beginning of the test. It is important for PWR SNF shipment after storage without opening DPC lids for pre-shipment inspection that the integrity of PWR SNF will be demonstrated through this test.

Therefore, Regulatory Standard and Research Department, Secretariat of Nuclear Regulation Authority (S/NRA/R) has developed and reviewed the analysis model to estimate the cladding temperature through measurement of the surface temperature distributions of the test container with the purpose for comprehension of stored SNF cladding temperature behavior that has major effects on the integrity of SNF during storage. The performance of the model was reviewed by comparing the analysis results to the measured temperature distributions of the test container in the preliminary heat transfer test with electric heaters.

2. Test program for long-term storage of PWR spent fuel

A time schedule of the PWR SNF storage test is shown in Table 1. A planning of this test and designing of the test container started in 2009, and the storage test with actual SNF is going to be commenced in 2016. In advance of the test, the heat transfer test was implemented by utilities with the purpose to comprehend heat transfer characteristic of the test container in the beginning of 2014. We carried out the tests to obtain material property of the test container components from 2011 to 2012; the obtained properties were used as the input data to the analysis model. The development of the analysis model was started from 2011 both analysis model for the heat transfer test and analysis model for the storage test were developed. The performance review and modification of the model by comparing the analysis results to the measured temperature distributions of the test container in the heat transfer test were conducted.

2.1 PWR spent fuel for the storage test

In the storage test, two SNF bundles are to be stored; 42.8 GWd/t SNF bundle is to be stored from the beginning of the test and 55 GWd/t SNF bundle will be added 10 years after the beginning of the test. The cooling time of 42.8 GWd/t SNF bundle is 22 years as of 2015 and that of 55 GWd/t SNF bundle will be 12 years as of 2025.

2.2 Test container

The outline drawing of the test container is shown in Fig. 1. Up to two 17×17 type PWR SNF bundle can be accommodated in the test container. The dimensions of the container are 5.2 m in total height 1.7 m in the shell external diameter and 2.1 m in the thermal insulator external diameter. To

shield gamma ray and neutron from the SNF bundles, required shielding thicknesses for each container part are guaranteed, and neutron shielding material is installed. And to maintain the SNF bundles subcritical, borated aluminum is used for basket spacer. In the heat transfer test and the storage test, thermal insulators are installed on the surface of the inner container and on the outer shell to raise SNF bundle temperature to the target value. In the initial stage of the heat transfer test which models the storage test with single SNF bundle stored and/or the storage test of single heating and/or single SNF bundle storing, thermal insulator is installed on the surface of the outer shell and the cavity of the container is maintained as a vacuum because the heating rate of the single SNF bundle is too small to raise the SNF bundle temperature to that in actual dry storage condition. In the second stage of the heat transfer test, the thermal insulator is removed. The ports for internal pressure monitoring, vent and drain are installed in the lid.

2.3 Heat transfer tests

To comprehend the heat transfer characteristics of the test container, two cases of heat transfer test were conducted using two mock-up heaters to simulate SNF bundle heating rates. In the storage test, single 42.8 GWd/t SNF bundle is stored from the start and 55 GWd/t SNF bundle will be added in 10 years after, the temperatures of the container and the mock-up heater were measured in the single fuel case (Case 1) and in the double fuel case (Case 2). One heater models SNF bundle geometry in detail (Heater-D), and the other is simplified (Heater-S). In Case 1 which simulated the initial stage of the storage test, the heating rate of 520 W was applied to model the heating rate of the 42.8 GWd/t SNF bundle. Since the heating rate 520W was not enough to raise the cladding temperature, internal pressure was kept very low (approximately 2 Pa). In Case 2 which simulated the 10 years after the beginning of the storage test, the heating rates of 440 W and 980 W were applied to model the heating rate of the 42.8 GWd/t SNF bundle and the 55 GWd/t SNF bundle respectively and internal pressure was kept at approximately 70 kPa. The heat transfer test conditions are shown in Table 2. Thermocouples were placed on the container and the heaters as shown in Fig. 2. A set of 123 thermocouples in total were attached to measure the temperatures of the test container and the heaters.

Each heater simulated only total heating rates of SNF bundle. An axial distribution of the actual SNF bundle heating rate was not modeled by the heaters. The Heater-D modeled SNF bundle geometry and dimension, but the major materials of heater pins modeling fuel rods were stainless steel (cladding) and oxidized magnesium (MgO, insulant). The heater pins were surface-treated to the emissivity of 0.92 (measured value). Thermal conductivity of MgO was approximately 9 W/m·K (measured value).

2.4 Material tests

In order to provide input data for temperature analysis, the material tests to obtain thermal properties (thermal conductivity and emissivity) of the test container component materials whose

properties are unavailable or unreliable in literature were conducted from 2011 to 2012. In the case of thermal conductivity, ceramic fiber used as inner insulator and resin used as neutron shielding material were subjected to the tests. In the case of emissivity, carbon steel used as lid and shell, and stainless steel used as basket were measured.

3. Development of analysis model

The analysis model has been developed to estimate stored SNF cladding temperature from the surface temperature distributions of the test container. This analysis model consists of computer codes and sets of input such as physical model, boundary conditions, computational grid, and material properties. The performance of the analysis model was reviewed by comparing the analysis results with the measured temperature distributions of the heat transfer test.

3.1 Computer codes

In this model, a thermal fluid dynamics analysis and radiation heat transfer analysis were coupled. A commercial CFD code ANSYS FLUENT [1] was used for thermal fluid dynamic analysis. A code named S-FOKS [2] developed by the NRA for high precision radiation heat flux calculation, was used for radiation heat transfer analysis. The S-FOKS receives the FLUENT calculation result of surface temperature distributions as boundary condition, then calculates surface radiation heat flux and feeds it back to FLUENT. Through iterative calculations, heat conduction, natural convection and radiation heat transfer of the test container are solved.

3.2 Thermal conductivity of homogenized fuel model

Since a SNF bundle consists of a numbers of fuel rods, it is difficult to calculate with actual geometry of horizontal cross section of SNF bundle model due to a limitation of computing capacity. For this reason, fuel assembly was modeled as homogenized solid. Separate calculations were made with an actual fuel assembly cross section model to derive equivalent thermal conductivities to the horizontal cross sections of the homogenized solid. Examples of the analysis results of cross sectional temperature distributions are shown in Fig. 3 and the calculated thermal conductivities are shown in Table 3. In Case 1 where the cavity of the container is vacuum state, since the effect of thermal conductivity is negligible, a temperature distribution of the fuel assembly cross section is not parabolic shape but flat and there is a sharp temperature gradient on the fringe of the fuel assembly. So, cross section of the fuel assembly model was divided into two parts, central part and outer part. An equivalent thermal conductivity is applied to central part and the equation of radiation heat transfer between parallel plates is applied to outer part. In Case 2 where the helium pressure is sufficiently high, the equivalent thermal conductivity of the homogenized solid is determined by the result of temperature distribution analysis using FLUENT and S-FOKS with 2-dimensional detailed fuel assembly model.

The axial thermal conductivity of homogenized solid is determined by volume averaging of thermal conductivity of each material.

3.3 Boundary conditions

In the calculation using FLUENT, temperature distributions of the outer shell surface of the test container was set as boundary conditions. These temperature distributions were set up based on the data measured by thermocouples attached on the outer shell, lid and bottom plate of the test container and the surface temperature of each cell was set by using bi-linear interpolation.

3.4 Computational grid

The computational grids for the analysis model used in FLUENT consisted of approximately 2.4 million hexahedral computational cells. The computational grids for test container are shown in Fig. 4.

3.5 Material properties

The values for thermal conductivities of following materials were taken from the literature or the test data listed:

- Stainless steel (basket, inner shell, lid, bottom plate and outer shell), carbon steel (shell): JSME Data Book: Heat transfer 5th Edition [3]
- Borated aluminum (basket separate plate): the data provided from the test container manufacturer
- Ceramic fiber (inner insulator) and resin (neutron shielding material): the measured data in the material shown in Table 4

The emissivity of stainless steel and carbon steel obtained from the measured data in the material test are shown in Table 5. Helium and air are treated as fluid; the specific heat, density, thermal conductivity and viscosity coefficient of the gasses obtained from the data listed in JSME Data Book: Heat transfer 5th Edition [3] and JSME Data Book: Thermo-physical Properties of Fluids [4].

4. Results and discussions

4.1 Cases and conditions of analyses

In advance of the heat transfer test, the preliminary analysis was conducted to evaluate the causes of the difference between measured and calculated temperature distributions. The models and the conditions of analysis were modified based on this evaluation.

4.2 Result of Case 1 (single mock-up fuel heating case)

4.2.1 Result of preliminary analysis

The preliminary analysis of Case 1 was conducted with the container surface temperature distribution shown in Fig. 5 as a boundary condition. The temperature distribution was set by bi-linear interpolations from the measured temperatures. The analysis results of temperature profiles

are shown in Fig.6 comparing with the measurements results. In this case, since the pressure in the test container was quite low (approximately 2Pa: measured value), the thermal conduction and the natural convection in the cavity between top of the basket and inner surface of the lid was negligible. Therefore, the axial heat transfer in the top region of the container was prevented by its low thermal conductivity and low convection because of the low pressure (approximately 2 Pa: measured value). At the underpart of the test container, since a ceramic fiber insulator layer exists, axial heat transfer was also disturbed significantly as with the case of the top region of the container. Consequently, as shown in Fig. 6 (a), the axial temperature distribution of the Heater-D is an axially symmetrical shape and has a peak at near the center height of the test container (cross section-A in Fig.2). The analysis result reproduced macroscopic characteristic of the actual temperature distribution and the temperature cross section-A agreed roughly with the measured data.

On the other hand, in the case of top and bottom of the Heater-D, the analysis results show 30ºC to 35ºC lower than the measured temperatures. According to Fig. 6 (b), the temperature difference between analysis result and measured temperatures of the central part at the cross section-A is within approximately 4ºC, while for the temperature distribution in radial direction, the analysis result showed parabolic shape whereas measured temperatures showed asymmetric shape with peak shift toward basket separate plate.

4.2.2 Result of verification analysis

In the verification analysis, following items of the analysis model were modified based on the evaluation to understand the gap between the preliminary analysis result and measured data

(1) Consideration of air natural convection in the gap between inner thermal insulator and shell
In the preliminary analysis, the effect of natural convection in the gap area was disregarded. In the verification analysis, fluid model was added to the analysis model so that the effect of the natural convection was able to be reflected to the analysis.

(2) Modification of equivalent conductivities for top edge and bottom edge of Heater-D
By reflecting detailed structure of top edge and bottom edge of heater, the equivalent thermal conductivities were set smaller.

(3) Modification of homogenized model for Heater-D
In the preliminary analysis, cross section of the Heater-D model was divided into two parts: central part and outer one. For each part, different equivalent thermal conductivities were used. The equation of radiation heat transfer between parallel plates was applied to outer part. This enables the analysis to model the emissivity difference between basket and basket separate plate to the temperature distribution.

(4) Modification of basket separate plate emissivity
The emissivity on the surface of basket separate plate was reduced from 0.15 to 0.04 (lower limit of aluminum emissivity data listed in literature [3]).

The comparison between the verification analysis result and measured temperature data is shown in Fig. 7. As shown in Fig. 7(a), the temperature difference between the analysis and the measured

temperature of top edge and bottom edge of the Heater-D decreased to 10ºC. As shown in Fig. 7 (b), the temperature difference between the result of analysis and the measured temperature data of central part of the Heater-D at the cross section-A decreased to 2ºC. The temperature distribution in the Heater-D shows that the peak shifted toward basket separate-plate as observed in measured temperature distribution.

4.3 Result of Case 2 (double mock-up fuel heating case)

4.3.1 Result of preliminary analysis

A preliminary analysis of Case 2 was conducted with the container surface temperature distribution shown in Fig. 8 as boundary condition. The temperature distribution is set in the same manner as 4.2.1. A comparison of the analysis result and the measured temperatures is shown in Fig. 9. In this case, since the helium pressure in the test container was approximately 70kPa, the thermal conduction and natural convection in the cavity between top of the basket and inside surface of the lid is effective. For this reason, axial heat transfer increased in the top of the inner shell compared to Case 1. Axial temperature distribution of the Heater-D is asymmetric shape which has a peak at a level lower than cross section-A. The analysis result reproduces macroscopic characteristic of the temperature distribution.

Fig. 9 (a) shows that the analysis results roughly agree with the measured data at the top of the test container. But at center height and lower part of the test container, inner shell temperature considerably exceeds measured data. The temperature at the center of the Heater-D at the cross section-A is 50ºC higher than the measured data. According to Fig. 9 (b), the analysis result of the radial temperature distribution of the Heater-D at the cross section-A has a parabolic distribution with a peak at center, while measured temperature shows flat distribution and the temperature at center was slightly lower than that of the outer part.

4.3.2 Result of verification analysis

In the verification analysis, the analysis model was modified as follows based on the results of consideration of the cause of the difference between the result of preliminary analysis and measured data.

(1) Consideration of air natural convection in the gap between inner thermal insulator and shell
    As with the Case 1, the effect of natural convection in the gap area was disregarded in preliminary model, but the fluid model was added to the verification analysis model so that the effect of the natural convection was able to be reflected to the analysis.
(2) Modification of homogenized model for the Heater-D bottom edge and emissivity of basket separate plate
    The same modifications as Case 1 were made.

As a result of the analysis with modified model the temperature of the inner shell at the center height of the test container (cross section A) notably decreased and the temperature difference between the analysis result and the measured data was reduced because of the consideration of air

natural convection. But at the inner shell, the difference between the analysis and the measured is still large. As shown in Fig. 6(a), such temperature difference also occurred in Case 1 in the lesser degree. It was attributed to unexpected large heat transfer occurred from the inner shell to the shell at the bottom part of the test container. Therefore, the result shown in Fig. 8 was reviewed and the potential heat transfer path was investigated. As a result, the contact areas of shell and four bosses attached around the bottom plate of inner shell were found as a potential heat transfer path. Since the smallest gap between the top surface of the bosses and inner surface of the shell is 1.5 mm, even slight misalignment of the inner shell with the height of approximately 4 m would cause the contact of the bosses to the shell. Furthermore, the temperatures of bottom plate near the boss were 70ºC in Case 1 and 120ºC in Case 2, whereas the temperature of the shell was 20ºC in Case 1 and Case 2. Making a prediction of the gap between the bosses and the shell under the temperature condition like this, the gap distances will be reduced to approximately 0.5 mm due to the thermal expansion of the bottom plate to indicate potential contact to the shell.

Based on above consideration, a follow-up analysis with the assumption that the contact of the four bosses with the shell was made and the result was that, as shown in Fig. 10, the temperature distribution at bottom part of the test container well agrees with the measured temperature distribution. However, according to Fig. 10 (b), the temperature of Heater-D center part at cross section-A is still approximately 35ºC higher than the measured temperature. It was found that the large difference between the analysis results and the measured data was caused by the significantly flattened temperature distribution of the measured data. Therefore, an effect was surveyed with the model of tentatively triplicated equivalent thermal conductivity of the entire axial length of heating part. As a result of this analysis, the temperature difference of the Heater-D center part at the cross section-A decreased to approximately 14ºC as shown in Fig. 11. Meanwhile, in this analysis, since the model was also modified with consideration to the gap between the basket and the side surface of the top gap above the Heater-S, the temperature difference of the analysis results and the measured data decreased at the top surface of the Heater-S compared to Fig. 10. On the other hand, as shown in Fig. 12, the radial temperature distribution of Heater-D at the bottom end (cross section-B2) is not in flat shape like that at the cross section-A, but parabolic shape as ordinarily expected. The same shape is observed at the top edge (cross section-B1). From these reasons, the flattening of temperature distribution as seen in the cross section-A can be said that it occurs only at local parts of the Heater-D. Since the temperature measurement points at the cross section-A is nearby the support grid of the heater pins, there is a possibility of the radial direction heat transfer via support grid. The effect of support grid on temperature distribution is described in 4.4.

4.4 Result of sensitivity analysis

Sensitivity analysis was conducted to confirm the effect of support grid on the temperature distribution of Heater-D. For this analysis two types of 3-dimension model for fuel assembly were used: a model without support grid and a model with support grid as shown in Fig. 13 (a) and (b)

respectively. Heat transfer of each model was simulated by using FLUENT code with the same conditions of Case 2. The effect of support grid to the shape of temperature distribution was investigated by comparing the calculation results.

The conditions of the simulation: material properties, radiation factors, and heat densities were same with the actual value of the Heater-D in the heat transfer test. The inner surface of basket of the test container was set as outer boundary of the model and its temperature was set at 170ºC. In these models, helium gas was treated as solid to ignore thermal convection of helium gas.

The results of the analysis are shown in Fig. 14 and Fig. 15.The temperature contours are compared at the center cross-section. The maximum temperature obtained from “with support grid model” was 0.9ºC lower than that from “without support grid model”, and flattening of temperature distribution was not confirmed. Consequently, it can be concluded as the support grid has no major effect on flattening of temperature distribution.

4.5 Summary of results from Case 1 and Case 2 tests

As a result of the comparative review of the analysis model, the cladding temperature of the stored fuel can be well predicted by measuring the surface temperature distributions of the test container. The review of the results of Case 1 and Case 2 are as follows.

Case 1

- The difference between calculated result by this model and the measured temperature is within 2ºC.
- In case of the storage test, this model will be able to predict the fuel cladding temperature with an uncertainty of 10ºC.
- As a precondition to the prediction, surface temperatures of the test container must be specified as boundary conditions with the same precision as the heat transfer test, and an uncertainty of decay heat and material properties must be excluded.

Case 2

- A significant flattening of temperature distribution in radial direction of Heater-D is observed.
- From the result of sensitivity analysis, it appears that support grid has low relevance to flatting of temperature distribution of Heater-D.
- In the heat transfer test, unexpectedly large heat transfer from the inner shell to the shell is presumed.
- Contact areas between inner-shell bosses and shell are assumed as a heat transfer path.
- A tripled equivalent thermal conductivity is tentatively input as a radial thermal conductivity of homogenized solid for a flattening of temperature distribution in radial direction of Heater-D.
- As a result of above modification, the temperature difference between the analysis results and the measured data of the Heater-D decreased to approximately 15ºC.

5. Conclusion

In advance to the storage test of PWR SNF bundles, an analysis model has been developed to estimate the SNF cladding temperature from the measured temperature distributions of the test container surface. The performance for the temperature estimation by the model was reviewed based on the measured data from the heat transfer test using electric heaters as mock-up fuel. The result of performance review showed that this model can estimate the cladding temperature of SNF bundle with uncertainty of approximately 10ºC in the first stage of the storage test with single SNF bundle stored under extremely low internal pressure. In the second stage of the storage test with double SNF bundles stored in helium atmosphere, the uncertainty of estimation is expected to be smaller than approximately 15ºC. From the sensitivity analysis results, it is understood that the support grid has low relevance to the observed flattening of temperature distribution in radial direction of Heater-D. Further study is needed in order to elucidate the root cause of flattened temperature distribution of Heater-D and to confirm the accuracy of temperature estimation by this model.

References

[1] ANSYS, Inc. Web page. http:/www.ansys.com/Products/

[2] Katayama, J. et. al., JNES-RE-Report Series, JNES-RE-2013-2017 "Improvement of Thermo-Fluid Simulation Code (1)," Japan Nuclear Energy Safety Organization, Tokyo, (2013).

[3] JSME Data Book: Heat-transfer 5th Edition, The Japan Society of Mechanical Engineers, Tokyo (2010).

[4] JSME Data Book: Thermophysical Properties of Fluids, The Japan Society of Mechanical Engineers, Tokyo (1983)

Table 1 Time schedule of PWR fuel storage test

	2009	2010	2011	2012	2013	2014	2015	2016
Planning and Designing	Planning Designing							
Heat transfer test		Determination of Measurement Point			Attachment of Thermocouple/ Setup of Test Container	Heating/Measurement of Temperature Distribution		
Material test			Data Measurement (Emissivity of Stainless Steel, Thermal Conductivity of Ceramic Fiber and Resin)					
Development of analysis model			Development of Input Data Computational Grid, Analysis Model		Test Analysis of Thermal Test /Test Analysis of Storage Test	Validation of Temperature Evaluation Model		
Storage test							Periodic Measurement of Surface Temperature	
Thermal analysis of storage test							Periodic Analysis Estimation of SNF Cladding Temperature	

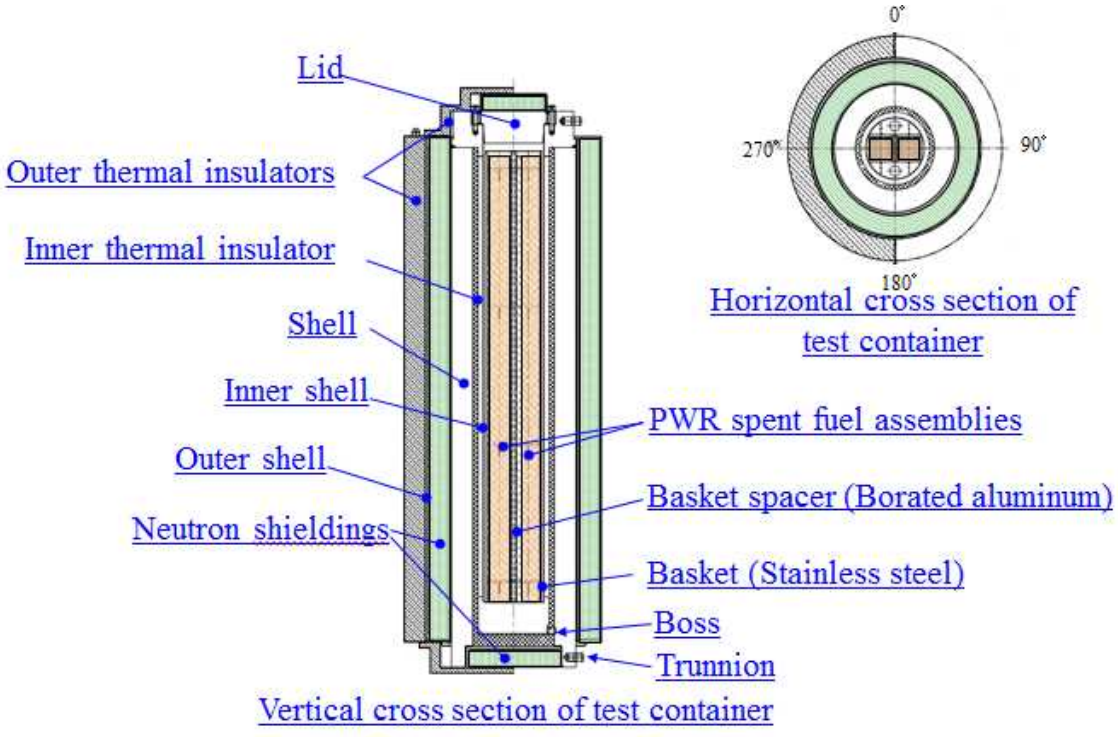

Fig. 1 Outline drawing of test container

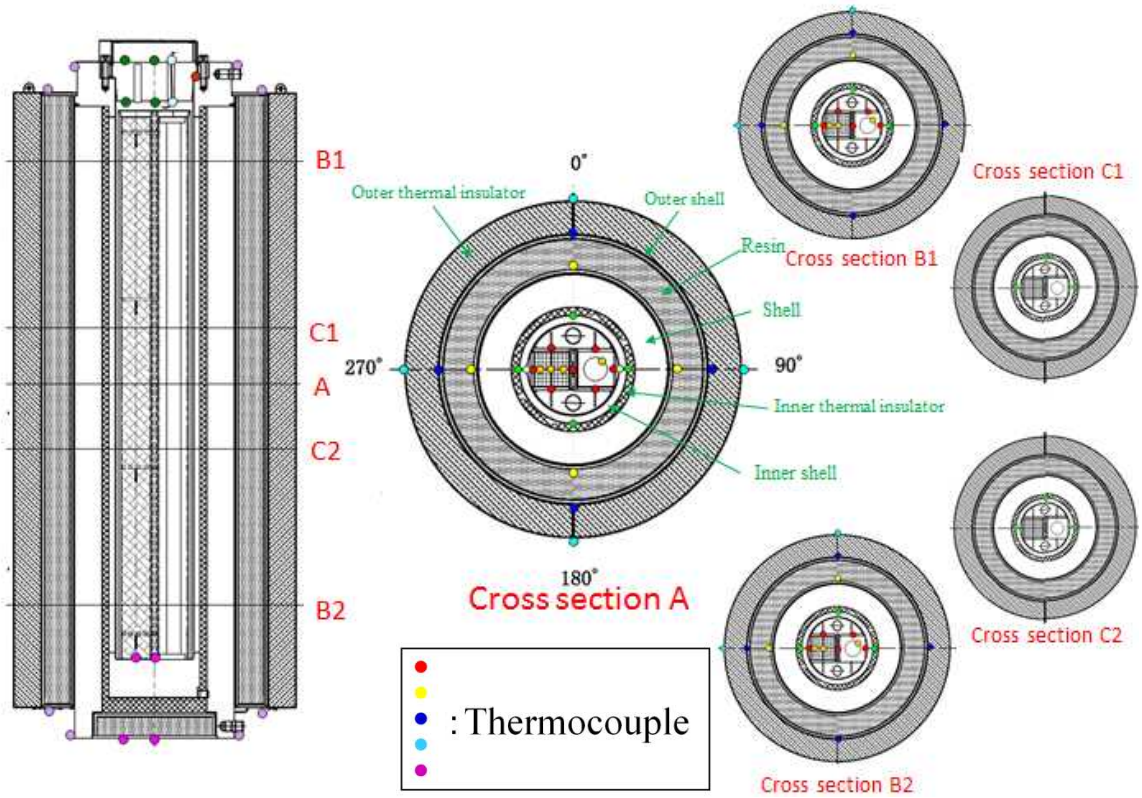

Fig. 2 Thermocouple placement

Table 2 Heat transfer test conditions

	[Case 1] Single mock-up fuel heating	[Case 2] Double mock-up fuel heating
Heat load	520W	1420W(440W+980W)
Container atmosphere	Rarefied Helium	Helium
Inner pressure	Approx. 2Pa	Approx. 70kPa
Outer thermal insulator	installed	—

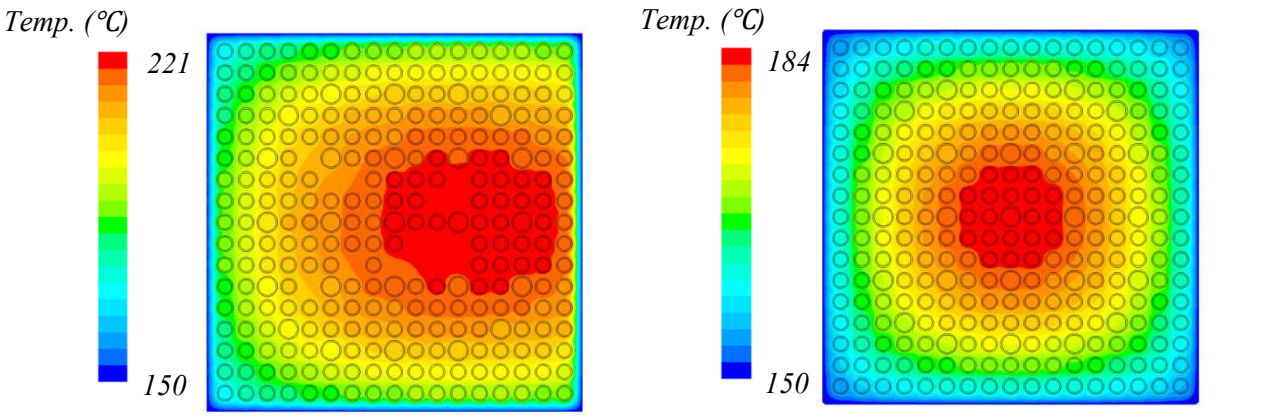

(a) 42.8GWd/t fuel assembly in Case 1 (boundary condition:150℃)

(b) 55GWd/t fuel assembly in Case 2 (boundary condition:150℃)

Fig. 3 Examples of temperature analysis results for SNF cross section

Table 3 Equivalent thermal conductivity of SNF cross section

Fuel cross-section mean temperature (ºC)	Equivalent thermal conductivity (W/m·K)		
	Case 1 42.8GWd/t fuel	Case 2 42.8GWd/t fuel	Case 2 55GWd/t fuel
-50	0.054	0.331	0.329
0	0.068	0.384	0.388
50	0.087	0.443	0.453
150	0.146	0.580	0.606
250	0.242	0.748	0.794

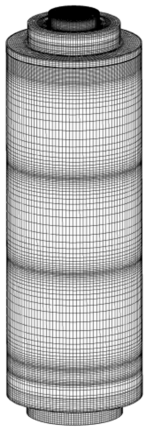

(a) Outer surface of test container

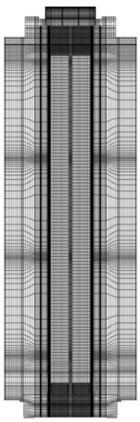

(b) Vertical cross section of test container (270°～90°)

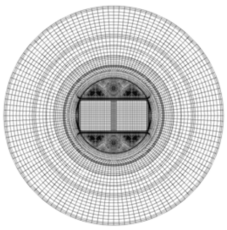

(c) Horizontal cross section of test container (center height of the test container)

Fig. 4 Computational grids for test container

Table 4 Thermal conductivity of ceramic fiber and resin

Temperature (ºC)	Thermal conductivity (W/m·K) Ceramic fiber
28	0.0285
101	0.0363
202	0.0478
301	0.0602

Temperature (ºC)	Thermal conductivity (W/m·K) Resin
35	0.884
83	0.829
141	0.742

Table 5 Emissivity of stainless steel and carbon steel

Temperature (ºC)	Emissivity	
	Stainless steel (rough surface)	Carbon steel
28	0.284	0.021
101	0.290	0.026
202	0.298	0.035

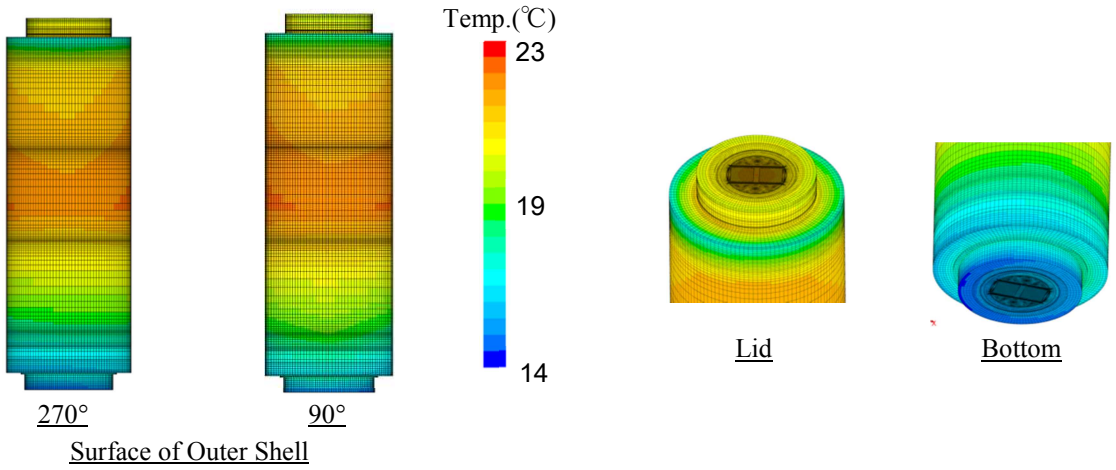

Fig. 5 Boundary condition of container surface in Case 1

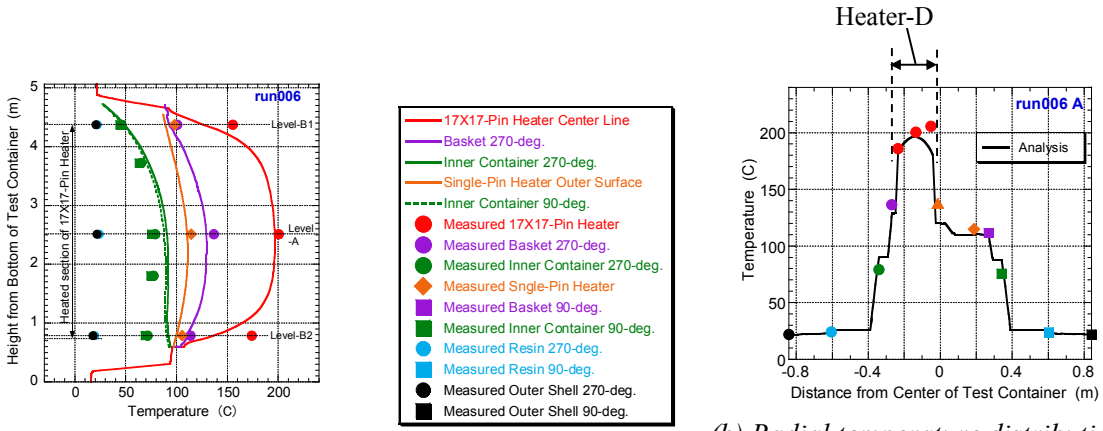

(a) Axial temperature distribution of test container

(b) Radial temperature distribution of test container (cross section-A)

Fig. 6 Comparison of preliminary analysis result and measured temperature distribution data of Case 1

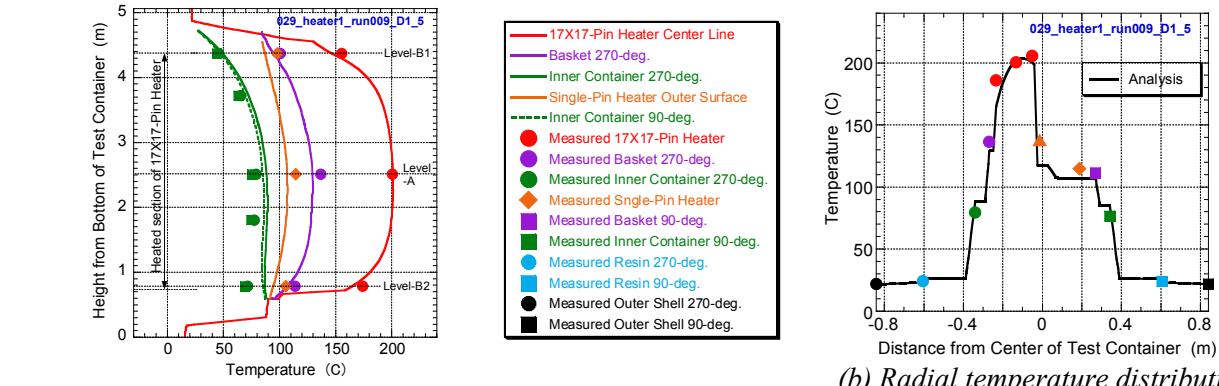

(a) Axial temperature distribution of test container

(b) Radial temperature distribution of test container (cross section-A)

Fig. 7 Comparison of verification analysis result and measured temperature distribution data of Case 1

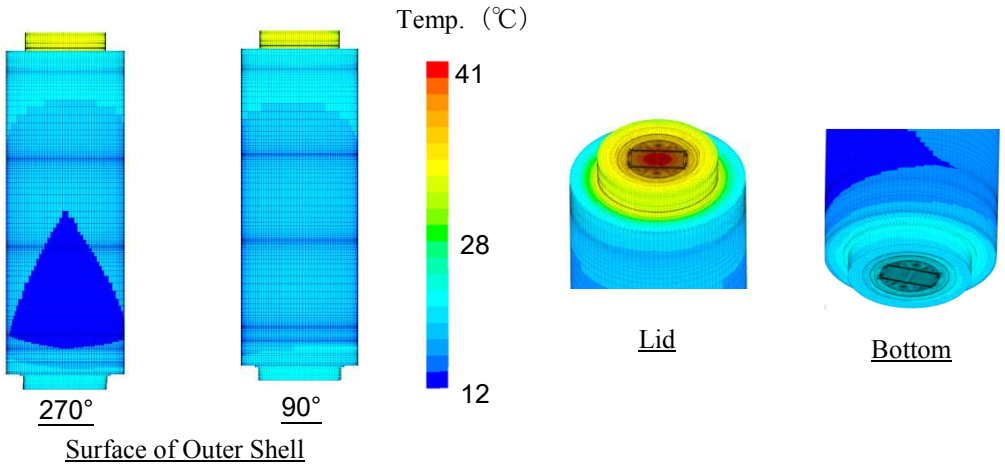

Fig. 8 Boundary condition of container surface in Case 2

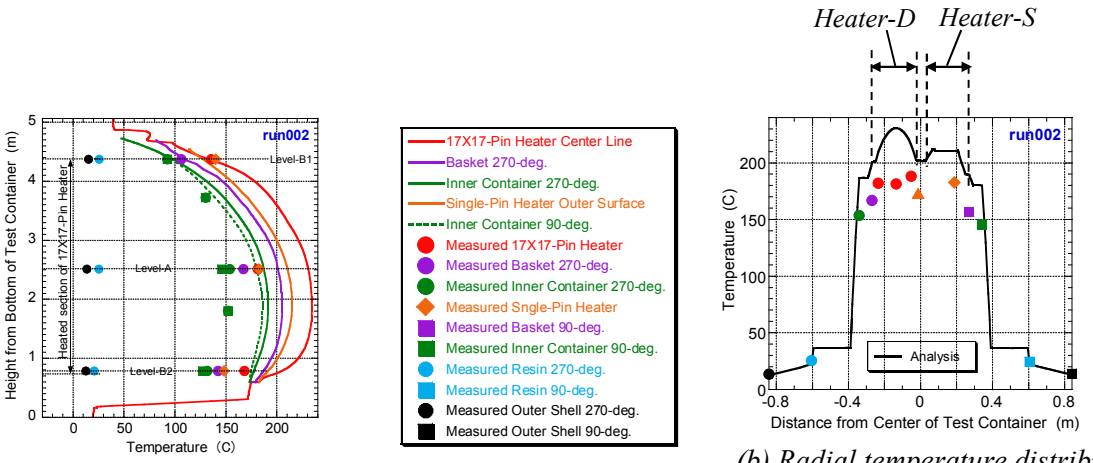

(a) Axial temperature distribution of test container

(b) Radial temperature distribution of test container (cross section-A)

Fig. 9 Comparison of preliminary analysis result and measured temperature distribution data of Case 2

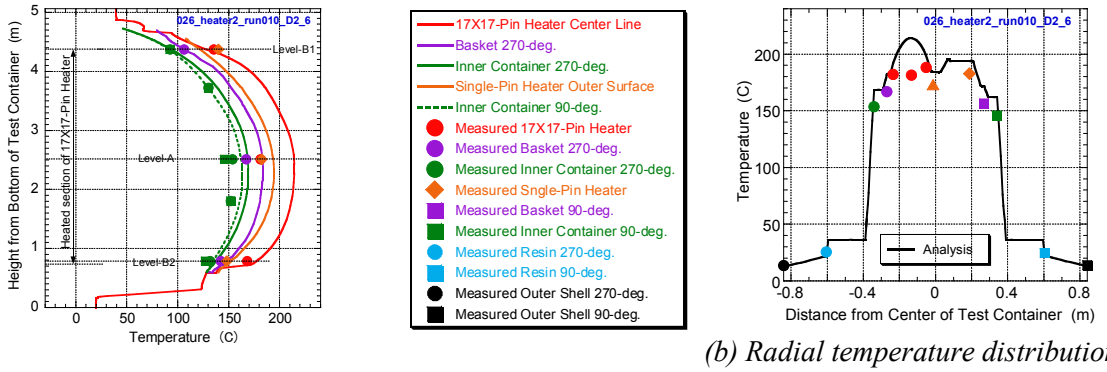

(a) Axial temperature distribution of test container

(b) Radial temperature distribution of test container (cross section-A)

Fig. 10 Comparison of verification analysis result and measured temperature distribution data of Case 2

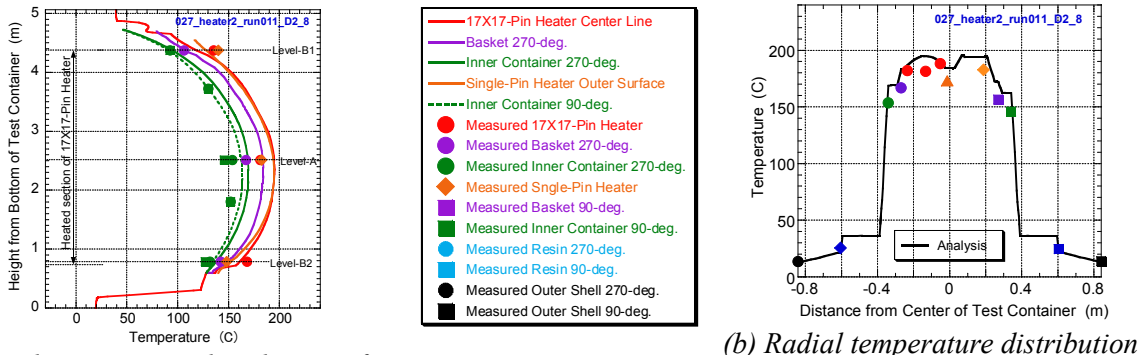

(a) Axial temperature distribution of test container

(b) Radial temperature distribution of test container (cross section-A)

Fig. 11 Comparison of verification analysis No.2 result and measured temperature data in Case 2

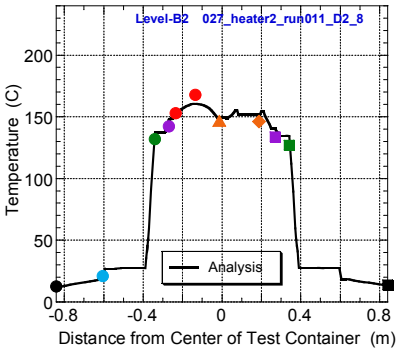

Fig. 12 Comparison of verification analysis result and measured temperature data at cross section-B2 in Case 2

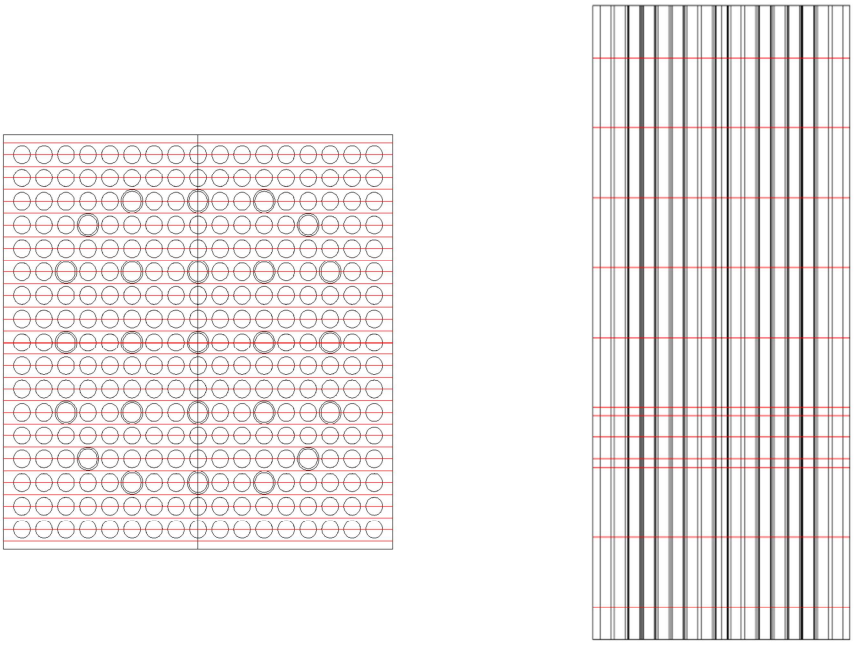

(a) Horizontal and vertical cross section of "without support grid model"

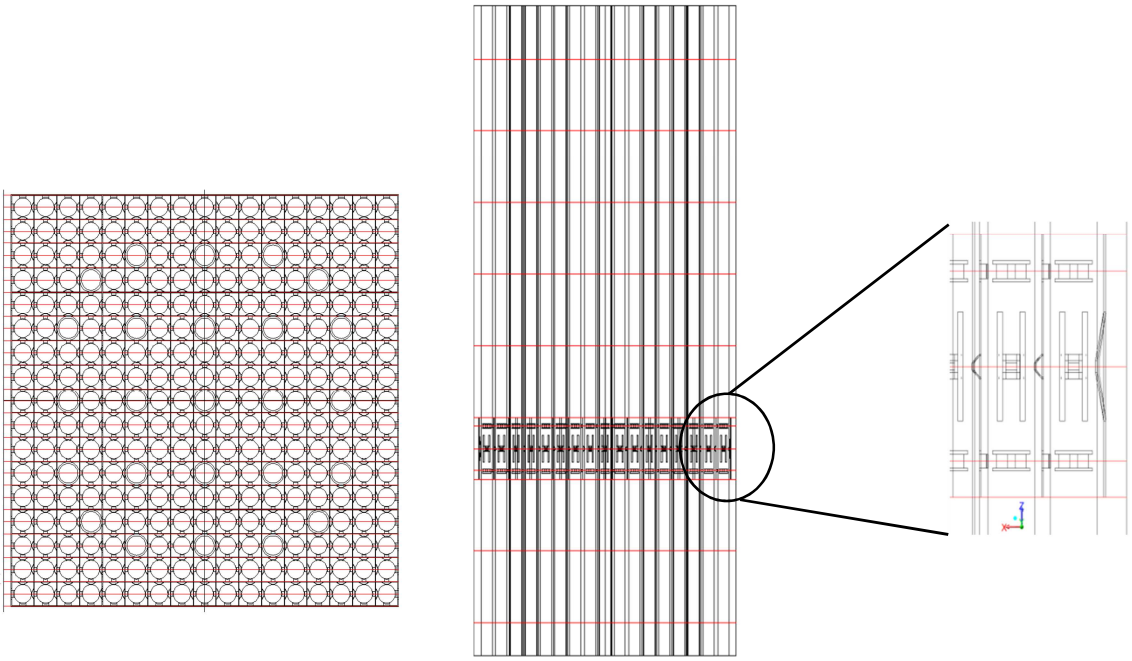

(b) Horizontal and vertical cross section of "with support grid model"

Fig. 13 Computational grids for sensitivity analysis

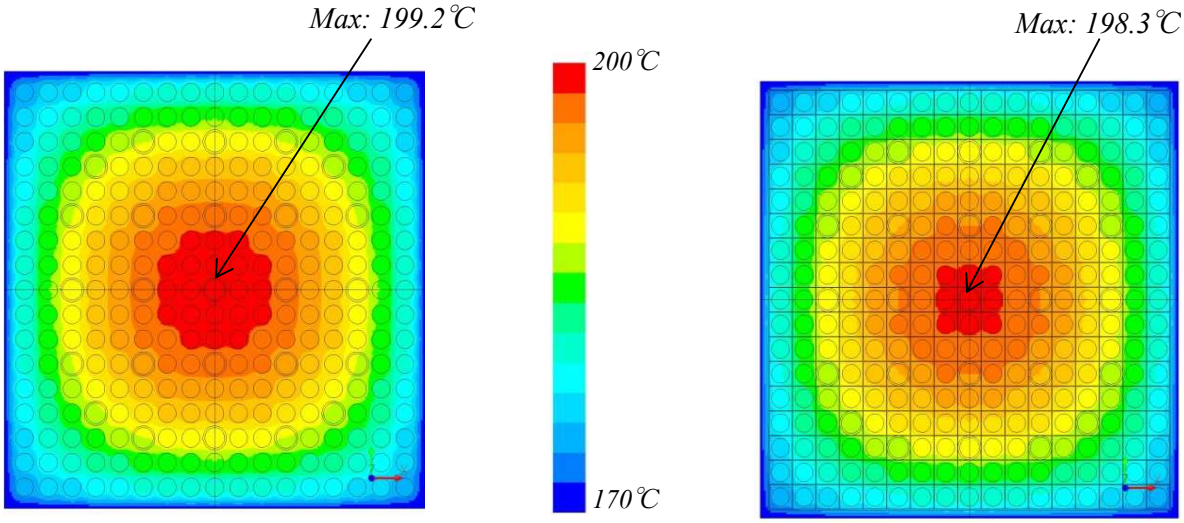

(a) Temperature contour of "without support grid model" *(b)Temperature contour of "with support grid model"*

Fig. 14 Comparison of temperature contour of "without support grid model" and "with support grid model"

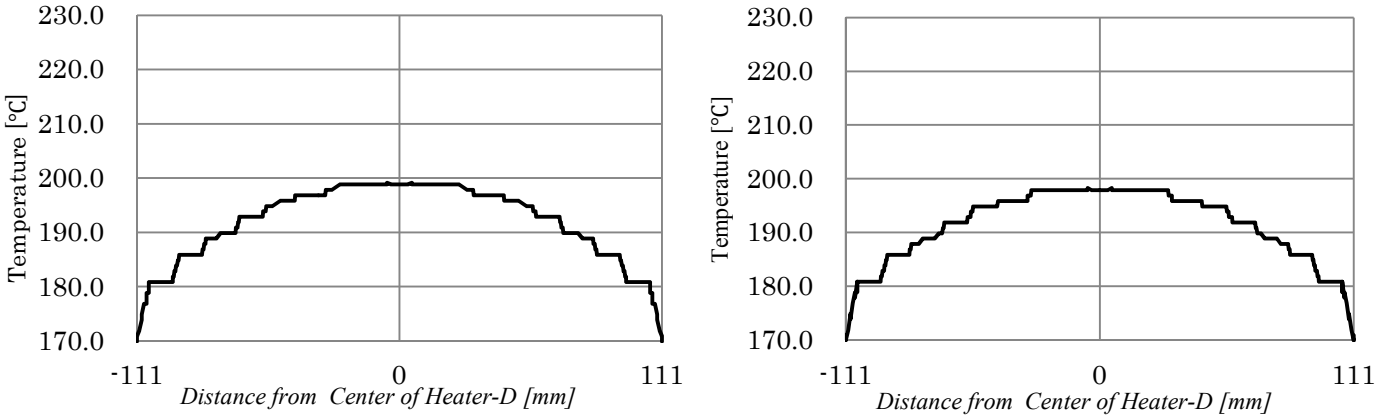

(a) Temperature graph of "without support grid model" *(b) Temperature graph of "with support grid model"*

Fig. 15 Comparison of temperature graph of "without support grid model" and "with support grid model"